University of Oxford

Honour School Of Physics

AO16: Trace Species and Aerosol Flagging with IASI Data

Candidate Number:
152785

Supervisors:
Dr. A. Smith
Prof. R. G. Grainger

A report submitted in partial fulfillment of the requirements for the degree of Master of Physics

in the Department of Physics

Word Count: 5251 + 763

Abstract

A method was developed for the manipulation of data from the Infrared Atmospheric Sounding Instrument (IASI), a Fourier transform infrared spectrometer mounted on the MetOp A and B satellites, to observe changes in target gases' column concentrations. Regions were selected that experienced episodic changes (for example, from the products of biomass burning). For each area a covariance matrix was constructed from measurements of the background excluding events of interest, combined with a measure of sensitivity (the Jacobian matrix) of the relevant gas, and applied to measurements of an anomalous event. This gave the estimated change in gas column mass from its "background" state. The effects of using different covariance matrices and Jacobians were investigated, with the most appropriate chosen for numerical analysis of signals. In the case of biomass burning, CO and C_2H_2 were the main gases whose raised concentrations indicate the event, while for volcano events SO_2, and pollution events NO were the main indicators. The decay time for the biomass burning CO plume observed in this work was around 20% of maximum per day, or around five days to decay completely. An SO_2 plume was observed in the area of interest near Australia after the eruption of the Puyehue-Cordón Caulle volcano in Chile. This was in agreement with other measurements taken around this time. Two other events, one over western Africa and the other over Europe were also investigated. The African signal was a biomass burning event and the Europe event was caused by pollution.

1 Introduction

Every year there are a number of naturally occurring events which cause problems for both local populations and regionally. For example, the Eyjafjallajökull eruption in Iceland in 2010 cost airlines $1.7bn [1], and the Mt. Pinatubo eruption in the Philippines in 1991 lowered global surface temperatures by 0.5 °C [2]. In the case of Eyjafjallajökull, a no-fly-zone was imposed around the ash plume to prevent aeroplane damage, investigated by Watts [3].

This report aims to develop a method to identify atmospheric pollution events such as biomass burning, industrial pollution and volcanic eruptions. In doing so it will address the question of "What are the principal gaseous perturbations associated with biomass burning, volcanic eruption and urban pollution events?" The work will also assess the sensitivity of the method to the vertical distribution of the gases as well as the natural variability of the atmosphere, including an analysis of the variability of the signal.

The method used in this report follows closely that of Walker et al. [4]. Forest fires are significant as they may account for up to 30% of global CO emissions [5]. The "Black Saturday" fires in South-Eastern Australia in 2009 were a major event [6], and are a focus of this study. The procedure is then applied to a variety of other events, including a burning plume over West Africa and a pollution episode over Europe. In the results section there is analysis of the constitution of the plumes, including identifying which gases are the best indicators for each event, along with how location can vary the proportions of each gas.

2 Background

2.1 The IASI

The Infrared Atmospheric Sounding Interferometer (IASI) instrument is a Michelson Interferometer mounted on the MetOp satellites, the first of which was launched in October 2006. Radiance spectra are measured, and from this a black-body temperature (BBT) spectrum can be calculated. The measured infrared (IR) range is 645–2760 cm^{-1} or 15.5–3.62 µm [7]. IASI covers almost 8,500 sequential wavenumbers in increments of 0.25 cm^{-1} which makes it a powerful tool for investigating absorption lines of gases with emission features in the IR.

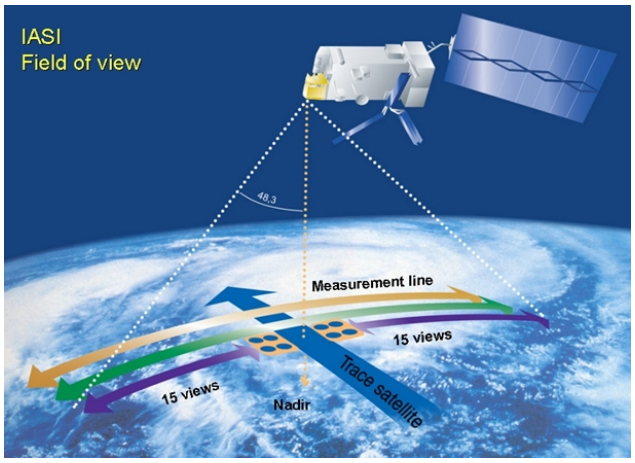

(a) IASI Field of View [8]

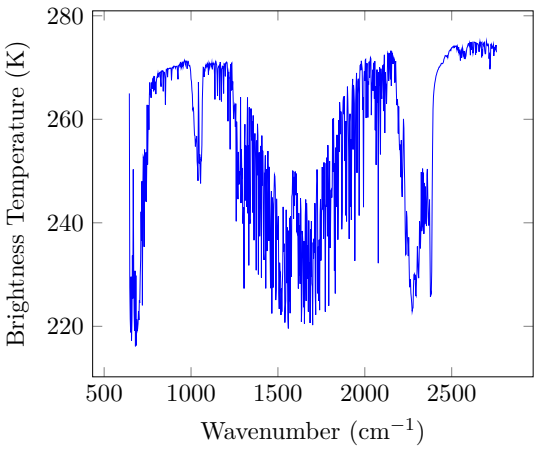

(b) An example BBT spectrum

Figure 1: Examples of the IASI field of view and a brightness temperature spectrum.

IASI is in a sun-synchronous polar orbit, providing readings at approximately 10:30 a.m. and p.m. local solar time every day. As the satellite moves down across the globe it sweeps out side-to-side to capture data, not just at the nadir but at small angles as well. The angle is determined such that one edge of a sweep down coincides with the opposite edge of the next sweep. Each reading gives the spectrum of a spot on the Earth of radius 12 km. This ensures almost total global coverage during a single day. This is shown in Fig. 1a: the far left hand side of this sweep will meet the far right hand side of the next sweep when not at the equator.

2.2 The Reference Forward Model (RFM)

The RFM is a radiative transfer model created by Dr. Anu Dudhia at the Physics Department at the University of Oxford [9]. Given the atmospheric conditions at various heights such as temperature, pressure and gas concentrations, the RFM generates a top-of-atmosphere radiance spectrum. This is either output as a radiance or a black-body temperature spectrum. Black-body temperature (BBT) is the theoretical temperature that a black body would be, given its radiance. Monochromatic radiance as a function of wavenumber and temperature is:

$$B_\nu(\nu, T) = \frac{2hc^2\nu^3}{e^{\frac{hc\nu}{k_B T}} - 1},$$

which can be rearranged to give:

$$T = \frac{hc\nu}{k_B} \frac{1}{\ln(\frac{2hc^2\nu^3}{B_\nu} + 1)}.$$

For each pixel and wavenumber there is a B_ν measurement and the BBT can be calculated. More details and explanation are available in Appendix A.

Figure 1b is a BBT spectrum for an atmosphere generated by the RFM. In the centre there is a large section of lower BBT. This corresponds to a large amount of absorption, in this case by water vapour. Surrounding this area are two areas of high, flat BBT. These are "window regions" of little or no absorption. Here the BBT measured is the temperature of the ground, in this case approximately 275 K. It is from the RFM that the Jacobian for each gas is generated.The Jacobian is a matrix which shows how each wavenumber varies with a change in the amount of gas in an atmosphere. In this particular case, the Jacobian for a single gas is:

$$\mathbf{K} = \left[\frac{\partial T_1}{\partial \tau}, \frac{\partial T_2}{\partial \tau}, \frac{\partial T_3}{\partial \tau}, ...\right]$$

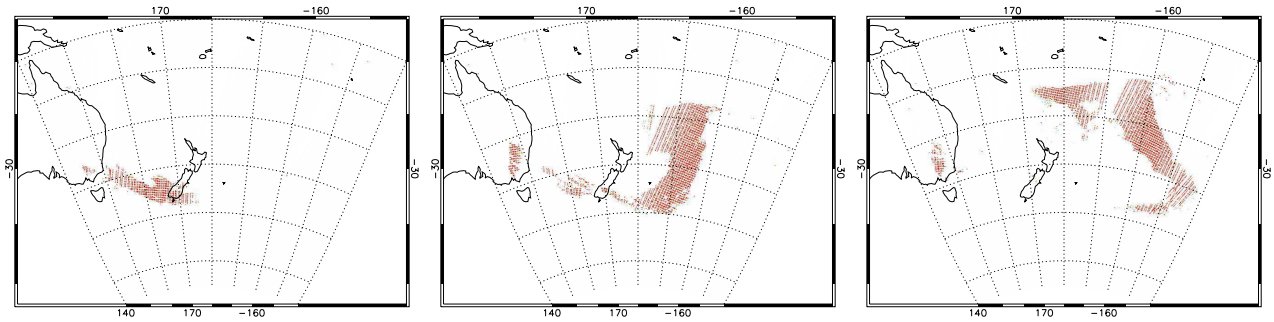

(a) Afternoon of 7th Feb 2009 (b) Afternoon of 8th Feb 2009 (c) Afternoon of 9th Feb 2009

Figure 2: A time series of the CO plume created by the Black Saturday bushfires in New South Wales, Australia in February 2009. These plots were created using the method described and shows a distinct CO signal. A full time series is available in Appendix B.

where τ is the column amount of gas by which the atmosphere is perturbed and each T_i are the BBT measurements at the ith wavenumber.

3 The Method

The radiance spectrum for each point is represented by a model atmosphere, plus extra contributions from errors:

$$\mathbf{y} = F(\tau, \mathbf{u}) + \epsilon_{\text{rnd}} + \epsilon_{\text{sys}} \tag{1}$$

where $\mathbf{y}$ is the measured BBT spectrum for the pixel chosen, $F(\tau, \mathbf{u})$ is the model atmosphere, namely the RFM, τ is the column mass of the gas to be analyzed and $\mathbf{u}$ is an estimate of all of the other parameters, such as temperature, pressure and other gases. In addition, ϵ_{rnd} is a random noise error contribution and ϵ_{sys} is a systematic error introduced by imperfect parameterisation of $\mathbf{u}$.

The model is linearized around a stationary point defined by a perceived normal state (that is, lacking the abnormal effects of the event to be studied):

$$\mathbf{y} - F(\tau_0, \mathbf{u}) = \mathbf{K}(\tau - \tau_0) + \epsilon_{\text{rnd}} + \epsilon_{\text{sys}}. \tag{2}$$

The Jacobian of the the gas, $\mathbf{K}$, is the change in BBT given some small change from the original amount. Instead of finding the errors associated with each part of the system, a matrix of covariance, $\mathbf{S}$, is used. $\mathbf{S}$ shows how the BBT at each wavenumber changes with variations in each other wavenumber, and therefore inherently takes into account the errors. It is constructed by taking data from the area of interest preceding the event, to find the natural variations. A baseline covariance can be calculated from these "normal" data points:

$$\mathbf{S} = \frac{1}{N-1}\sum_{i=1}^{N}(\mathbf{y}_i - \overline{\mathbf{y}})(\mathbf{y}_i - \overline{\mathbf{y}})^{\mathrm{T}}. \tag{3}$$

Each point is combined with itself to find how each of its wavenumbers vary with each other, then divided by the number of points give a mean variation. If two wavenumbers have a particularly high covariance then it is likely that they are both affected by changes in the same gas. Conversely, a low covariance means they are more independent. $\mathbf{S}$ and $\mathbf{K}$ are combined to create the gain matrix, $\mathbf{G}$:

$$\mathbf{G}^{\mathrm{T}} = (\mathbf{K}^{\mathrm{T}}\mathbf{S}^{-1}\mathbf{K})^{-1}\mathbf{K}^{\mathrm{T}}\mathbf{S}^{-1}. \tag{4}$$

The inverse of the covariance matrix is used so as to give a greater weight to the more independent (low covariance) terms. This is then used to find the offset of gas column mass from the linearisation point, $\tau - \tau_0$:

$$\tau - \tau_0 = \mathbf{G}^{\mathrm{T}}(\mathbf{y} - \overline{\mathbf{y}}). \tag{5}$$

It is $\tau - \tau_0$ which is plotted on the maps throughout this report. In each case red corresponds to a large positive offset is a sliding scale down to white for no offset.

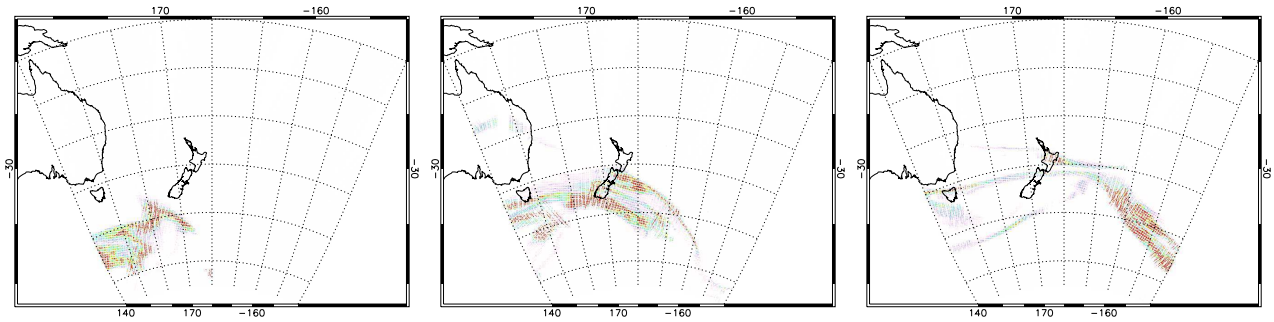

(a) Afternoon of 10th June 2011 (b) Afternoon of 11th June 2011 (c) Afternoon of 12th June 2011

Figure 3: Time series of the SO_2 plume from the Puyehue-Cordón Caulle eruption in June 2011. The plume moves very quickly across the sky from West to East. This figure shows that the method works, not only for the forest fire but for other events too.

In calculating the change in gas column mass it is possible to use one of two variants on the above method. In the first, each gas is considered separately and the method models changes in each gas independently of the others. It is possible that even if a gas is not present, the model suggests a signal. In the second, all gases are considered together and the likelihood of ghost signals is reduced. Due to this, the probability of measuring false positives is greatly reduced, and more reliable signals detected. Therefore, the combined matrix method is used.

4 Preliminary Results

4.1 Forest Fire

By applying this procedure CO, C_2H_2 and C_2H_4 were identified as displaying a signal. Gases that did not show a signal either were not perturbed or their change was within the natural variability of the atmosphere. See Appendix C for maps of all of the gases. Figure 2 shows a time series of the days succeeding the Black Saturday forest fires in New South Wales, Australia in 2009. Plotted here is the change in gas column mass, effectively showing where the gas produced by the forest fire is going. The carbon monoxide cloud is clearly tracked across the sky as it moves over New Zealand and starts to dissipate in the South Pacific. Now a picture can be built up of which gases are detectable in the plume and which are not. This enables the characterization of plumes depending on their makeup and hence the material being burned can be estimated. This is investigated more throughout the report.

4.2 Another Event over Australia

On the 4th of June 2011 there was a large eruption of a volcanic complex in Chile, Puyehue-Cordón Caulle [10]. This was an event which created a gas and ash cloud which moved across the whole of the southern hemisphere. Given that the eruption is a fundamentally different event, a different mixture of gases is expected. A few days after the recorded eruption there is a large signal of sulphur dioxide (SO_2), as shown in Fig. 3. The plume is moving rather quickly, indeed after three days the plume has all but passed through the region of study. This shows that this method works generally, not just for a forest fire event.

4.3 Comparing Covariance Matrices

The set of data which was used to train the covariance matrix affects the magnitude of the signal. For example, if in the training data there is negligible variation in CO levels, any increase in gas will give a signal, but a large natural variation will suppress a small potential signal. Therefore it is important that ap-

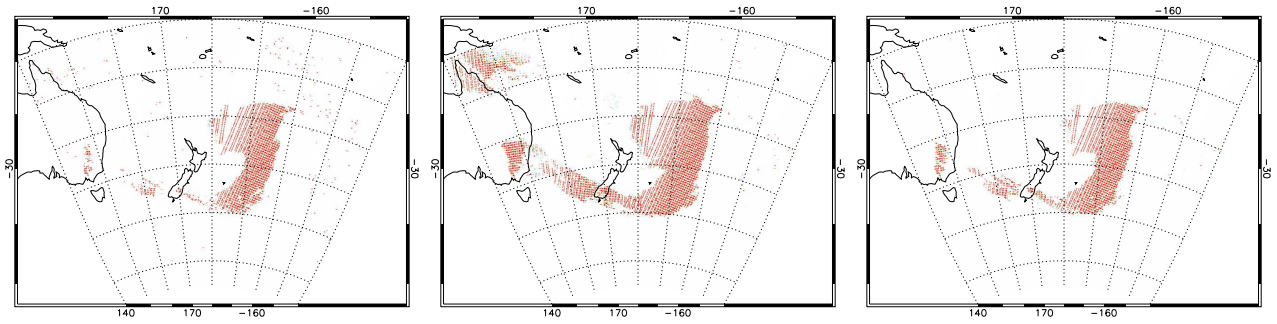

(a) West of dateline (b) East of dateline (c) Both sets

Figure 4: A comparison of various covariance matrices. Each of these were constructed using different data. The first uses training data from the West of the International Dateline, the second from the East and the third combines data from both. The training data used greatly affects the signal measured. In general, more data gives a more reliable baseline so the matrix constructed from the combined data is used.

propriate data with which to train the matrix is chosen.

Three covariance matrices were used, using data from the West, East and the combination of both sets of data. The western side contains a portion of Australia and the entirety of New Zealand. Given that both of these countries have large cities and industry, there is bound to be CO emissions from cars, industry and ships . In comparison, there is negligible landmass on the eastern side. The contribution from land-based emissions is eliminated and the lesser effect of oceanic CO is left.

Figure 4 shows the plume represented in Fig. 2b using covariance matrices trained on the three different sets of data mentioned above. The covariance matrices for each area give appropriate results for the areas on which they were trained. However, applying the eastern matrix to data containing Australia gives the false positives seen in the North West corner of the map. This is where the model starts to break down: where inappropriate parameters are given there will be errors in the output. The final image shows the plume using a covariance matrix created by combining the sets of data from both sides of the International Dateline. This forms a more reliable covariance matrix and reduces the noise that might infiltrate the data. Much of the "tail" region of the plume is still visible and the false positives in the North West corner of the map are completely cut out. It gives a much clearer picture of the plume and henceforth this is the covariance matrix used.

4.4 Comparing Jacobians

The biggest uncertainty in this approach is the location of the gas within the atmosphere, and hence the height profiles affect the Jacobians significantly. This has been quantified by investigating three potential vertical distributions. The first Jacobian (V1) is formed using a perturbation of 1% at around the tropopause level of approximately 10 km in a triangular fashion, the second (V2) is a 1% deviation across the whole atmosphere up to 20 km and the third (V3) is a triangular perturbation over a very wide range of heights, from ground level to 20km. The different atmospheric profiles of each Jacobian means that each is more sensitive to gas at particular heights. For example, the first focuses on CO at tropopause level, while the second and third extend well into the stratosphere. Figure 5a shows how each Jacobian is constructed, with the height profiles described above.

How does the Jacobian used affect the end result of the mass of the plume? In each case the plume mass was found and averaged over.

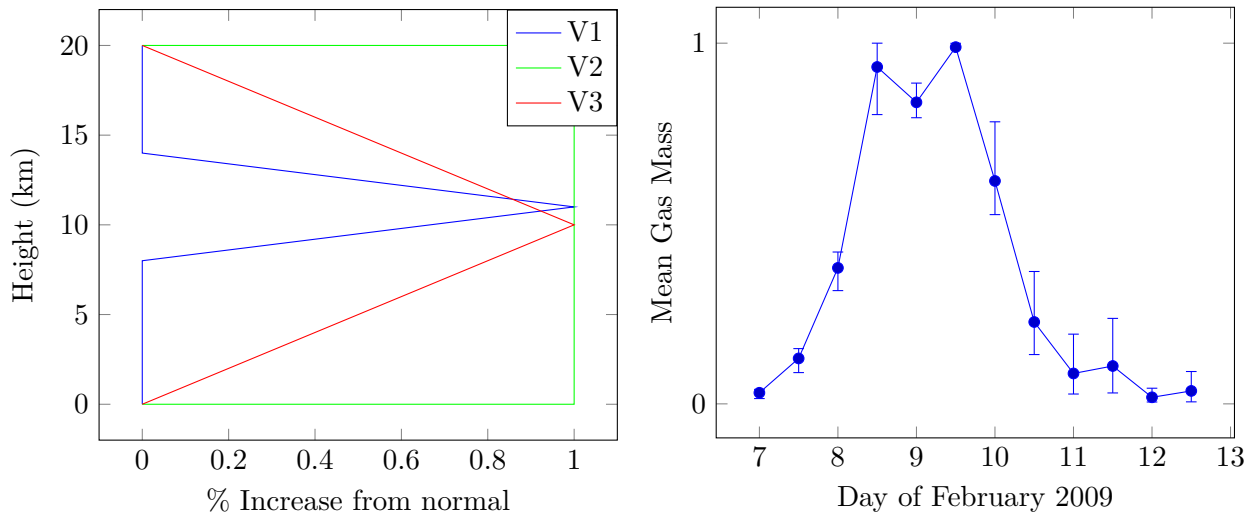

(a) Jacobian Height Profiles

(b) Normalized mass of plume over time

Figure 5: Analysis of the effects of using different Jacobians. Each of the Jacobian "versions" displayed here use a different height profile, showing the perturbation from the normal atmospheric levels of each gas that is used. This corresponds to different levels of sensitivity of each Jacobian to changes in gas amount at said heights. For example, V1 will be particularly sensitive to changes in gas at approximately tropopause height. The second graph shows the normalized mass of the CO plume as a mean of the signals from each of the three Jacobians. At the height of the plume there is a large amount of divergence, indicating the extent to which the Jacobian used affects the model.

This is the plot shown in Fig. 5b. The data from each calculation was normalized such that the peaks are at the same height. After the peak there is significant divergence, especially in the four data points on the 10th and 11th. This highlights the significance of the effects of using different Jacobians in the model. Additionally, at high concentrations the Jacobians become more inaccurate and the spread could result from this. The RMS deviations from the mean for these data points are all approximately 10% of the maximum. This error is also evident from the error bars on the line chart. The significant deviations from the mean when different Jacobians are used indicate that absolute results for the masses of the plumes calculated throughout should be taken cautiously.

Due to the fact that it can be generated automatically from the RFM and includes sensitivity for the entire height profile, the V3 form of the Jacobian is used.

4.5 Cross-Contamination

It should be noted that this method is by no means perfect. It relies on the channels affected by the Jacobian of each gas. There is a possibility of an overlap in said channels, given how many channels certain gases occupy. Figure 6 shows tables containing cross-contamination calculations for both the forest fire and volcano events. From these tables, along with knowledge of which gases are to be expected, it can be suggested which gases are real signals and which might be relics from other signals. The calculation multiplies the Jacobian value at each wavenumber for two gases and gives the total. Appendix D shows the normalized Jacobians from which these are calculated.

4.5.1 Forest Fire

Carbon monoxide is the main signal: it is clearly a legitimate signal, given its strength in the biomass burning event. It does not seem to have any overlap with any of the other

Gas	C_2H_2	C_2H_4	CCl_4	$ClONO_2$	CO	HCN
C_2H_2	-	0	0.39	0.57	0	0.88
C_2H_4	-	-	0.01	0.01	0	0
CCl_4	-	-	-	6.58	0	0.12
$ClONO_2$	-	-	-	-	0	0.11
CO	-	-	-	-	-	0
HCN	-	-	-	-	-	-

(a) Interference metric for forest fire gases

Gas	C_2H_6	$ClONO_2$	CO_2	F_{12}	NO	SO_2
C_2H_6	-	4.77	0.8	0.23	0	0.85
$ClONO_2$	-	-	1.39	0	0	0
CO_2	-	-	-	0.21	1.04	0.62
F_{12}	-	-	-	-	0	2.36
NO	-	-	-	-	-	0
SO_2	-	-	-	-	-	-

(b) Interference metric for volcano gases

Figure 6: Metrics for the cross-contamination between different Jacobians for particular gases for both the forest fire and volcano events. A higher value indicates a greater overlap between the Jacobian of the relevant gases. In the forest fire event, C_2H_2 overlaps with CCl_4, $ClONO_2$ and HCN. In the volcano event, C_2H_6 overlaps with $ClONO_2$, and SO_2 overlaps with F_{12}. The contamination suggests that some of these gases might be relics from other gases.

gases. However, there are also large amounts of the short hydrocarbons C_2H_2 and C_2H_4. C_2H_4 is clear of the other Jacobians, but C_2H_2 has a large overlap with both $ClONO_2$ and CCl_4 in the region around $750\,cm^{-1}$. Both of these gases are relatively unexpected in biomass burning events given the presence of chlorine, so it is very possible that these are contaminant signals. There is also a large overlap with HCN, a gas which is less clearly a contaminant given that hydrogen, carbon and nitrogen are all prevalent in plant material. Looking at Fig. 7a, the $ClONO_2$, CCl_4 and HCN time signals follow the form of the C_2H_4 signal very closely. This supports the claim that these are contaminant signals and that there are not actual plumes of these two gases emanating from the forest fire. Conversely, the signals for CO and C_2H_4, two gases believed to be greatly independent, have very different forms. The CO signal stays high for a long period of time, showing that it takes a long time to disperse. C_2H_4 on the other hand drops off very quickly, decaying by a factor of ten over one day. The fact that these gases act in separate ways lends credence to their being legitimate signals.

From these observations CO, C_2H_2 and C_2H_4 are the legitimate signals, whereas $ClONO_2$, CCl_4 and HCN are contaminants. This is in agreement with the expected products of biomass burning [11].

4.5.2 Volcano

For the volcanic event SO_2 is the main signal. From the Jacobian table in Fig. 6 SO_2 overlaps with F_{12}. There is also an overlap between C_2H_6 and $ClONO_2$. Looking at the time series plot in Fig. 8a, F_{12} follows SO_2 and $ClONO_2$ follows C_2H_6 very closely in form, supporting the claim of contamination.

As the plume moves in and out of the frame very quickly, it is tough to reliably estimate decay time. Purely from the Jacobian plots and a cursory look at the form of the time series for each gas, it seems that SO_2, C_2H_6 and NO and CO_2 are the proper signals, and $ClONO_2$ and F_{12} are contaminants. As with the biomass gases, this is in agreement with other observations [12].

Now that the factors affecting the output of the model have been looked at, and appropriate input parameters like covariance matrix and Jacobian have been chosen, each event can be numerically analyzed. There are also indicators of which gases should be present.

5 Analysis of Gases Detected

5.1 Forest Fire

Carbon monoxide has been used as the chief flagging gas for biomass burnings. This is not the only gas which is emitted during a forest fire: there are many hydrocarbons present [11]. Figure 7a shows the mass of carbon monoxide contained in the plume over the days succeed-

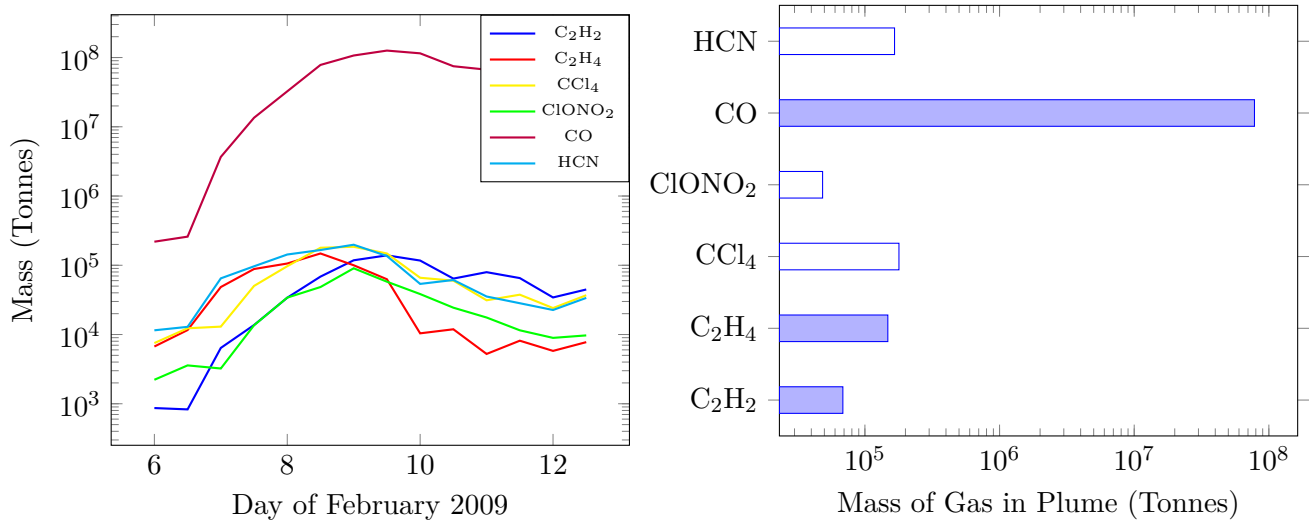

(a) Plume mass of many gases

(b) Bar plot of all gases for 8th February 2009

Figure 7: Gas comparison data for the forest fire plume. The plume grows in size very quickly after the start of the event, and takes a long time to decay. The ratios of gases show that forest fires are characterized by high levels of carbon monoxide and short hydrocarbons. The unfilled columns represent possible contaminant gases.

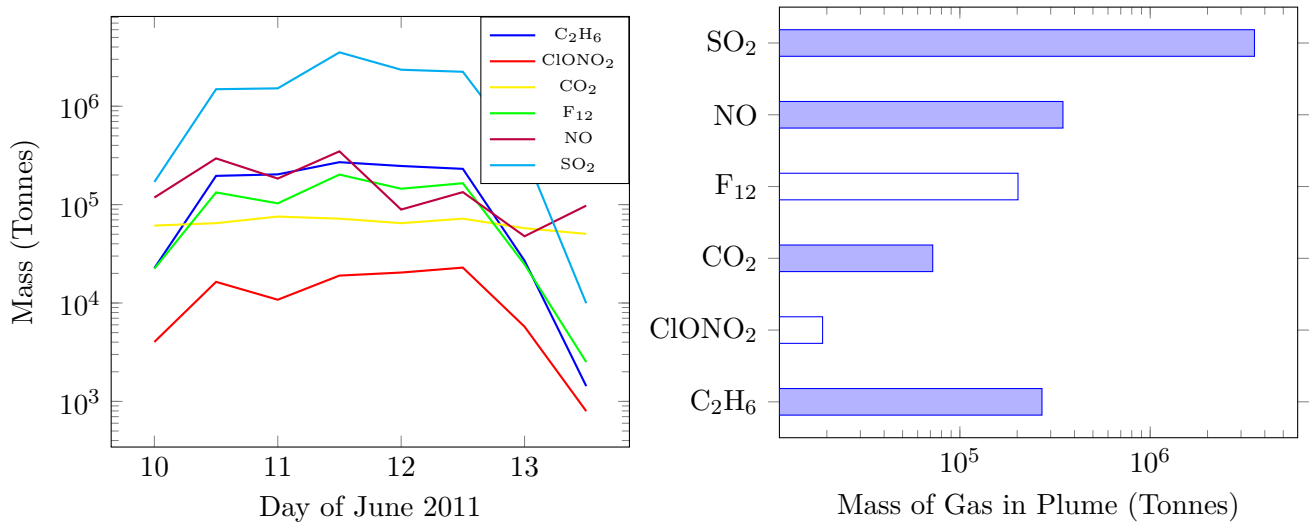

(a) Plume mass for many gases

(b) Bar plot of all gases for the 11th June 2011

Figure 8: Gas comparison data for the volcano plume. The change in amount of SO_2 is not as pronounced as the CO plume from the forest fire but is still significant. Volcanic eruptions are characterized mainly by SO_2. The unfilled columns represent possible contaminant gases.

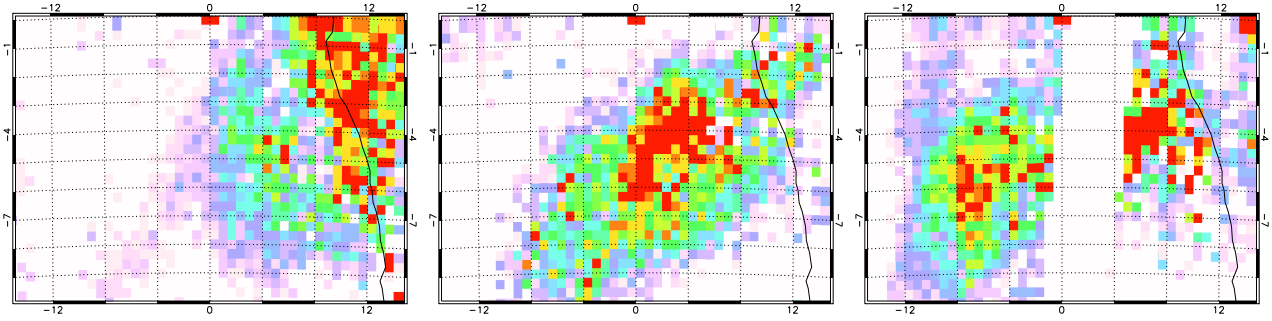

(a) Morning of 14th January 2010 (b) Morning of 15th January 2010 (c) Morning of 16th January 2010

Figure 9: Time series of the CO plume from biomass burning off the western coast of Africa in January 2010. This event is less distinct and is a rather continuous process. Therefore, each box is the mean of the pixels contained therein which shows a signal moving across towards the South West. There is an orbit of IASI missing in the third map, however the movements of the plume are still evident.

ing the event. As the plume grows there is a clear maximum, followed by a drop as it dissipates over the West Pacific Ocean. Analysis of the time series for the other minor gases shows that the CO drop is relatively slow. Both CO and C_2H_2 decay approximately 20% of their maxima per day.

Figure 7b shows the prevalence of a multitude of gases for the plume for the afternoon of the 8th February 2009, the same time as the Jacobian and covariance comparison maps. Carbon monoxide is the most common gas emitted, followed by C_2H_2 and C_2H_4. The suggested contaminant gases are included for completion. From the proportions of the constituent gases, a forest fire is characterized by especially high levels of CO and some C_2H_2. Additionally, the area of the plume can be estimated. Given that a pixel represents a circle of radius 12 km, the size of the plume on this day is approximately 1.72×10^6 km^2.

5.2 Volcano

Analysis of the gas constituency in Fig. 8 reveals a different makeup to the forest fire event. The largest of the signals is SO_2, followed by C_2H_6 as the next most perturbed gas. There are also lower levels of carbon dioxide and some other minor gases. As with the forest fire, there is a plot of how the plume changes with time. The cloud moves in and out of the area of measurement completely in four days from the 10th to the 14th so the decay due to dispersion and breakdown cannot be reliably measured.

5.3 Africa

On the western coast of Africa there is a huge amount of biomass burning all year round. This is anything from slash and burn forestry to burning rubbish [13] [14]. The particular area of interest in this case is just south of the equator, off the coast of Gabon down to Angola. A signal should be present and analyzable here. The aim of this section is to identify the gas distribution of this signal and characterize the plume.

It should be noted that the covariance matrix used in this section is not constructed from data in this area. The land surrounding the data points introduces a lot of variability which is not expected over the ocean. This includes temperature variations which are much higher over land. Additionally, this was an event which lasted many months; indeed it was a roughly continuous process. Data from a completely different time of year would have to be taken if no data from during the event was to be included. This introduces many other factors, such as seasonal changes, and is hence unsuitable. The covariance matrix was constructed

using data taken from the area to the West of this map, off the coast of Brazil. It included only ocean-based measurements and was taken at the same latitude and time of year so as not too stray too far from the natural variability which occurs in the area of interest.

Additionally, the mass of CO plotted in Fig. 10a should be taken cautiously given that some data is missing. On the 16th January an orbit of data from IASI which bisects the plume is not present. This is most likely due to corruption or improper reading of data. Unfortunately this means that the quantitative results will not be accurate, but the relative results of the proportions of gas to each other should be representative.

Figure 9 shows a carbon monoxide plume off the western coast under the horn of Africa. While the signal is not very clear, indeed there is a lot of noise, there is a clear progression of the plume towards the South West. Analysis of the gas constitution of the plume, shown in Fig. 10, indicates that this event is quite similar to that of the forest fire over Australia, the biomass burning event. This is characterized by high levels of CO and short hydrocarbons. The bar chart shows the masses of each gas relative to CO for this event, with the Australian amounts alongside. Possible reasons for the change in the relative amounts could be due to different biomass materials being burned. South-Eastern Australia, considered "Temperate Forest", releases smaller proportions of the shorter hydrocarbons relative to the Africa event, classed as "Tropical Savannah" [11]. This agrees well with the the relative amounts in Fig. 10. Indeed, at this time of year there is a peak in the amount of biomass being burned in North Africa [13] [14]. The speed of the plume is estimated at 420 km per day. Comparing this to the speed of the Australian plume, 3200 km per day, the Australian plume is a lot faster. Due to the fact that there is a clear CO plume and presence of the other minor gases similar to the Australian forest fire event, this is a biomass burning event.

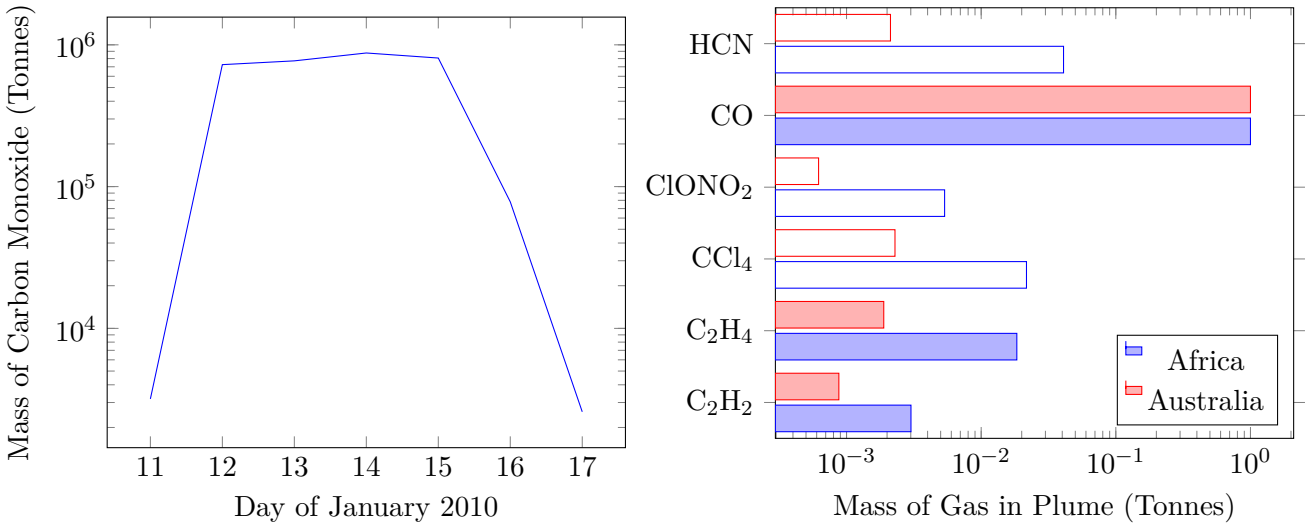

(a) West Africa Plume Mass of CO

(b) Bar plot of all gases for 14th January 2010

Figure 10: Gas comparison data for the event off the coast of Africa. There is a sharp increase in atmospheric CO followed by a drop made sharper by the lost data. The bar plot compares the gas ratios for the Australian and African events, normalized to CO. The African plume contains a lot more of the minor trace gases relative to the Australian plume, which has vastly more CO. This could, however, be a remnant of the covariance matrix for the Africa event, which was difficult to construct. The unfilled columns represent possible contaminant gases.

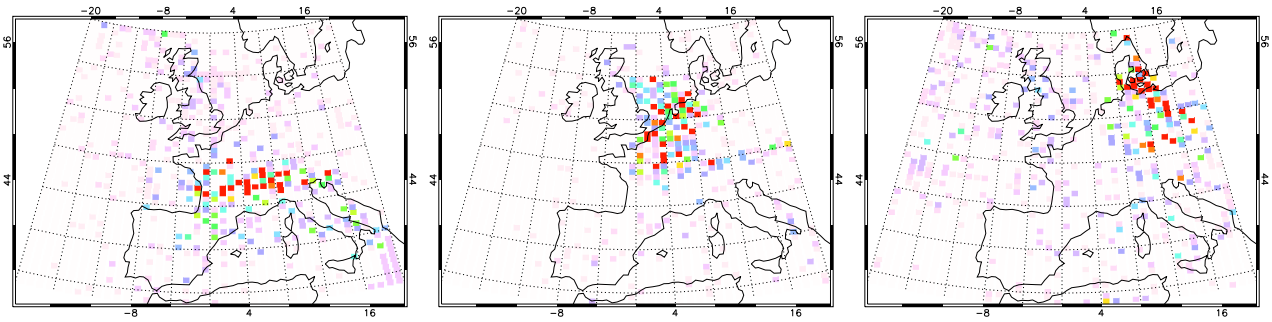

(a) Morning of 3rd April 2014 (b) Morning of 4th April 2014 (c) Morning of 5th April 2014

Figure 11: Time series of NO pollution across Europe in April 2014. Though the signal is noisy there is a clear movement of the signal towards the North and East. Like the African plot each box is the mean of the pixels contained within it. There were smog and pollution warnings for the 4th April in the South East of the UK, which corresponds to the cloud being in that area at that time.

5.4 UK

Given the high population density and industry levels of Europe, there is often high levels of pollution. This is especially prevalent during a "blocking high", a high pressure weather system which can sit above an area, resulting in little wind and high temperatures. These blocking highs prevent the dispersal of pollution through the movement of air and hence a signal may be present, however weak. The work in this section aims to find an indicator gas for this type of event.

As with the African signal, it should be noted that for this event the covariance matrix was built using specially selected data. The objective was to measure a pollution signal, therefore data with as little pollution as possible was needed for the covariance matrix calculation. Therefore, data was taken over twenty six Sundays in 2014 over the summer period. Sundays were chosen as it is often a day of closure for industry and many more cars are off the road on the weekend. Even with this covariance matrix the signal is somewhat weak, showing that the mass of gases produced by pollution is much smaller than the output from the forest fire and volcano events.

On the 4th of April there were pollution warnings across the UK, ranging from 7 out of 10 in London to even a 10 out of 10 in East Anglia [15]. This was due to large amounts of Saharan dust and pollution from industry in central and southern Europe, combined with a high pressure system preventing their dispersal. Figure 11 shows the movement of an NO signal across Europe in April 2014. On the 4th April there is a large signal over the South East of the UK, indicating high levels of pollution. This agrees well with the pollution warnings issued for this day. Given the dispersed nature of the signal and the fact that there are few pixels which show a distinct signal, it is impossible to quantitatively analyze the properties of the signal with any confidence. However, the speed of the plume is approximately 600 km per day. This is similar to the speed of the African signal.

Given the different relative amounts of gases in this event it is in a class of its own, neither a biomass burning nor a volcano-like event.

6 Conclusion

This report has documented the successful building and testing of a method to reliably detect and analyze signals taken from IASI to measure the change in gas column mass. Jacobians were generated from the RFM, combined with the covariance matrix from the relevant area, and the existence of a plume was determined for various events. The central question of "What are the principal gaseous

perturbations associated with biomass burning, volcanic eruption and urban pollution events?" was answered: biomass burning events were characterized as containing much CO and C_2H_2, and volcano events containing predominantly SO_2. This allowed the suggestion that the Africa event was biomass burning. The Europe signal contained much NO and a little SO_2, quite similar to the volcano but a distinct source.

There are a few avenues that continuations of this project could take. First, it would be very useful to find a stronger pollution signal which could be numerically looked at. This would allow for a better analysis of the constitution of the plume. Second, it would be beneficial to build covariance matrices with vastly more data. This would reduce the noise significantly and allow for a clearer detection of any plume. Finally, building up a tool which could automatically scan for and flag an event, including characterizing, would be very useful. This would allow for a near real-time detection and provide analysis.

References

[1] BBC, "Flight disruptions cost airlines $1.7bn, says IATA." 21 Apr 2010, last accessed 16 Mar 2015.

`http://news.bbc.co.uk/1/hi/business/8634147.stm`

[2] U. S. Geological Survey, "The Cataclysmic 1991 Eruption of Mount Pinatubo, Philippines." 28 Feb 2005, last accessed 16 Mar 2015.

`http://pubs.usgs.gov/fs/1997/fs113-97/`

[3] P. Watts, Ash detection and characterization in IASI data, *MPhys Masters Project*, 2012

[4] J. C. Walker, A. Dudhia and E. Carboni. An effective method for the detection of trace species demonstrated using the MetOp Infrared Atmospheric Sounding Instrument. *Atmos. Meas. Tech.*, 4, 1567-1580, 2011.

[5] D. V. Malia, J. C. Lin et al. Impacts of upwind wildfire emissions on CO, CO_2, and $PM_{2.5}$ concentrations in Salt Lake City, Utah. *J. Geophys. Res. Atmos.*, 120, 147-166.

[6] The Age, "Counting the terrible cost of a state burning", 2 Feb 2009, last accessed 03 Apr 2015.

`http://www.theage.com.au/national/counting-the-terrible-cost-of-a-state-burning-20090208-811f.html`

[7] CNES, "Infrared Atmospheric Sounding Interferometer." Last accessed 16 Mar 2015.

`http://smsc.cnes.fr/IASI/GP_instrument.htm`

[8] What is IASI? Last accessed 16 Mar 2015.

`http://www.eumetsat.int/website/home/Satellites/CurrentSatellites/Metop/MetopDesign/IASI/index.html`

[9] RFM User Manual. Last accessed 16 Mar 2015.

`http://eodg.atm.ox.ac.uk/RFM/index.html`

[10] NASA, "Puyehue-Cordón Caulle." Last accessed 16 Mar 2015.

`http://earthobservatory.nasa.gov/NaturalHazards/view.php?id=50862`

[11] S. P. Urbanski, Wei Min Hao, S. Baker. Chemical Composition of Wildland Fire Emissions. *Developments in Environmental Science*, 8, 79-107, 2008.

[12] USGS, "Volcanic Gases and Their Effects". 11 Jun 2010, last accessed 12 Apr 2015.

`http://volcanoes.usgs.gov/hazards/gas/index.php`

[13] G. Robert, M. J. Wooster, E. Lagoudakis. Annual and diurnal African biomass burning temporal dynamics. *Biogeosciences*, 6, 849-866, 2009.

[14] C. Liousse, B.Guillaume et al. Updated African biomass burning emission inventories in the framework of the AMMA-IDAF program, with an evaluation of combustion aerosols. *Atmos. Meas. Tech.*, 10, 9631-9646, 2010

[15] BBC, "UK air pollution: How bad is it?". 2 Apr 2014, last accessed 16 Mar 2015.

`http://m.bbc.co.uk/news/uk-26851399`

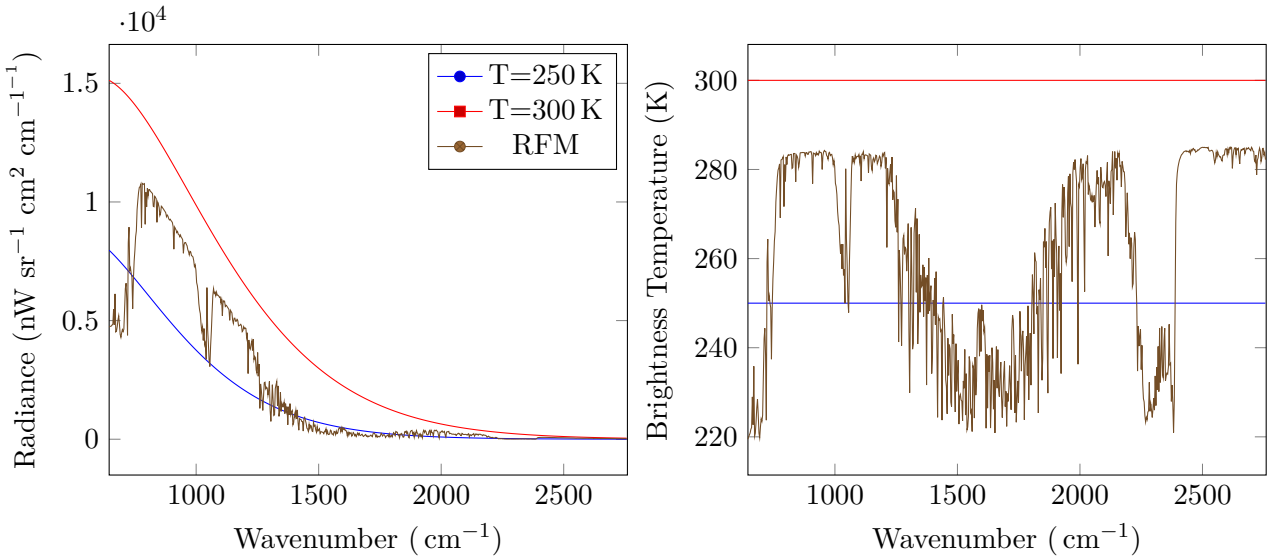

(a) Planck function.

(b) Brightness Temperature.

Figure 12: The spectral radiance and brightness temperature for two temperatures of the Planck function and an atmosphere generated using the RFM.

A The Radiance Equation

Here is the radiance equation again:

$$B_\nu(\nu, T) = \frac{2hc^2\nu^3}{e^{\frac{hc\nu}{k_B T}} - 1}$$

where ν is wavenumber, T is temperature, h is Planck's constant, c is the speed of light and k_B is Boltzmann's constant. The spectral radiance for a particular wavenumber and temperature is a measure of the amount of energy emitted per unit surface area per unit time in the region $[\nu, \nu + \delta\nu]$. It is also known as Planck's Law. Figure 12a shows the Planck function for two different temperatures as well as an output from the RFM. The Planck functions are idealized spectra, without any absorption from gases in the atmosphere. Conversely, there are many significant deviations from a smooth line for the RFM spectrum. This is indeed due to absorption patterns from gases in the atmosphere.

The Planck functions of different temperatures never cross, so each wavenumber has a unique temperature associated with its spectral radiance. This is known as the Brightness Temperature (BBT). For the generated spectra, as there is no deviation from the Planck function, the BBT will just be the temperature used to generate the spectrum. However, for the RFM spectrum, due to the absorption and the resulting deviation from the Planck function, the BBT will vary drastically. This is shown in Fig. 12b.

The deviations from the Planck function are much more clear in this form. There are areas of little absorption, where the BBT is flat and high, and areas of high absorption, where there are large negative troughs. For example, in the region around 1000 cm^{-1} there is a large trough corresponding to lots of ozone absorption. This is evident from the Jacobian for ozone, shown in Appendix D. Coarsely, a deeper trough would correspond to more ozone absorption, created by the presence of more ozone in that area. It is these deviations that the method identifies and draws out.

B Full Time Series of Plume

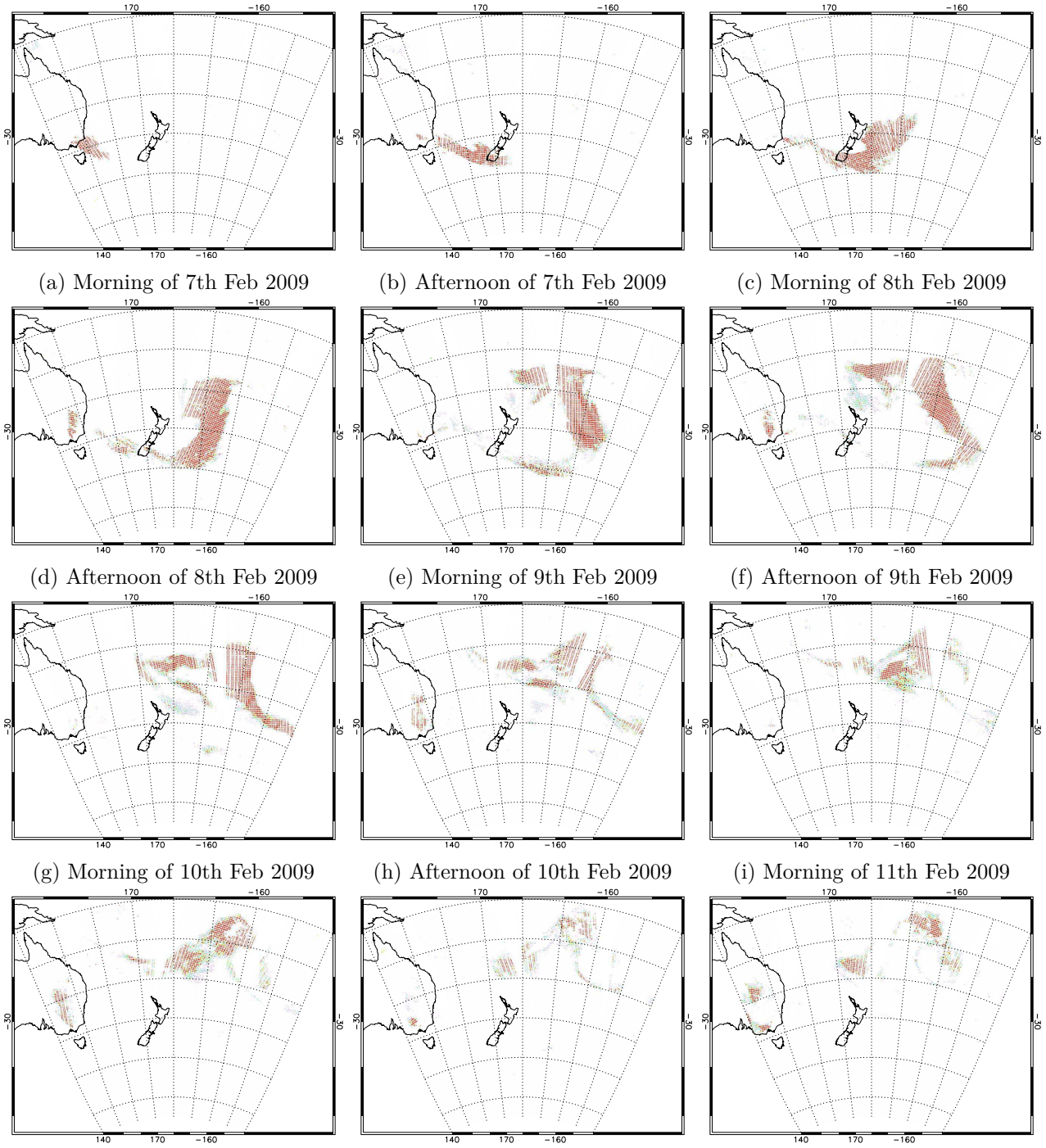

(a) Morning of 7th Feb 2009 (b) Afternoon of 7th Feb 2009 (c) Morning of 8th Feb 2009

(d) Afternoon of 8th Feb 2009 (e) Morning of 9th Feb 2009 (f) Afternoon of 9th Feb 2009

(g) Morning of 10th Feb 2009 (h) Afternoon of 10th Feb 2009 (i) Morning of 11th Feb 2009

(j) Afternoon of 11th Feb 2009 (k) Morning of 12th Feb 2009 (l) Afternoon of 12th Feb 2009

Figure 13: The full time series of the CO plume created on Black Saturday over Australia and the South Pacific in February 2009

C All Black Saturday gases

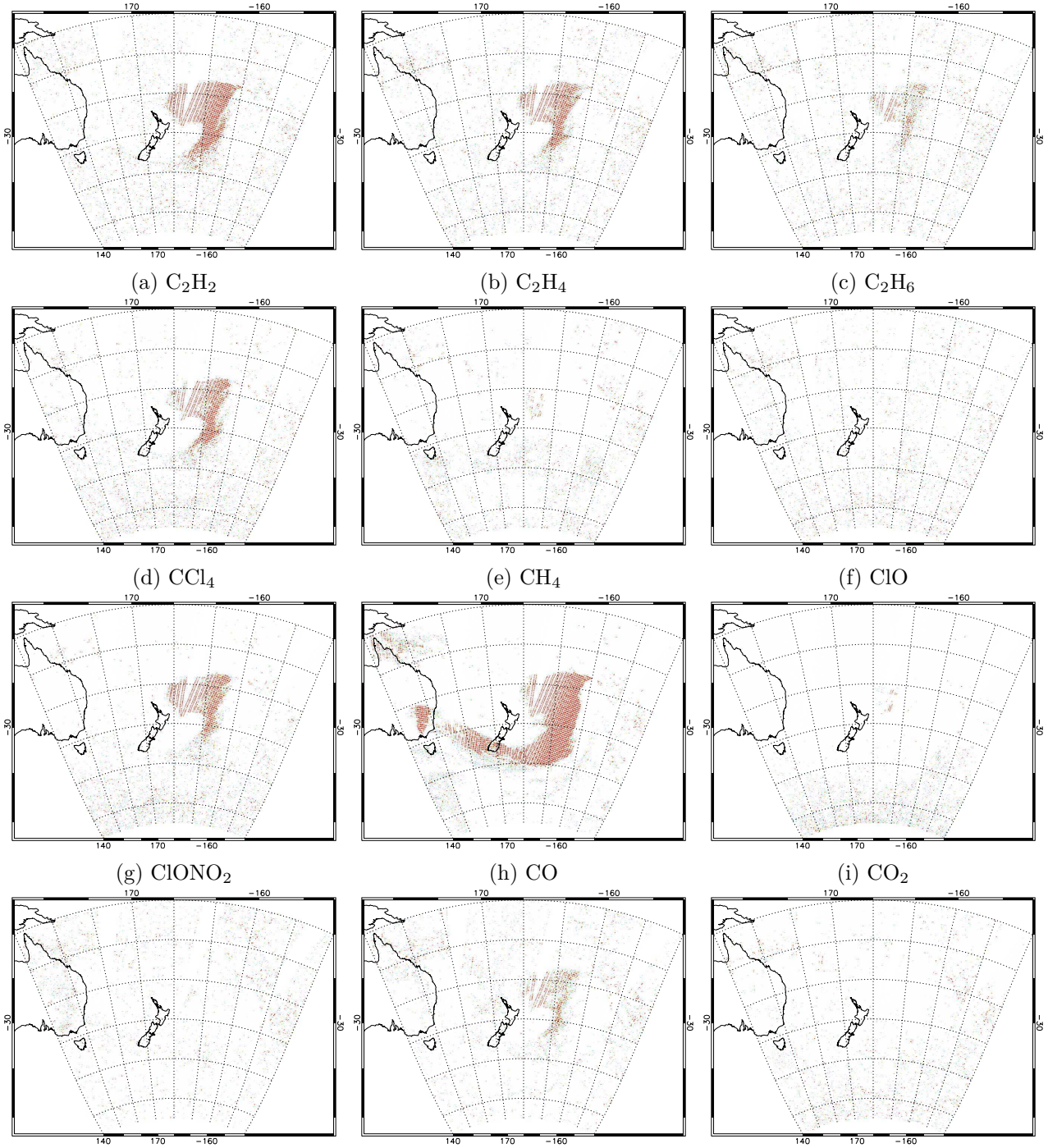

(a) C_2H_2 (b) C_2H_4 (c) C_2H_6

(d) CCl_4 (e) CH_4 (f) ClO

(g) $ClONO_2$ (h) CO (i) CO_2

(j) F_{11} (k) F_{12} (l) F_{14}

Figure 14: Maps of the plume on the afternoon of the 8th February 2009 for many different gases.

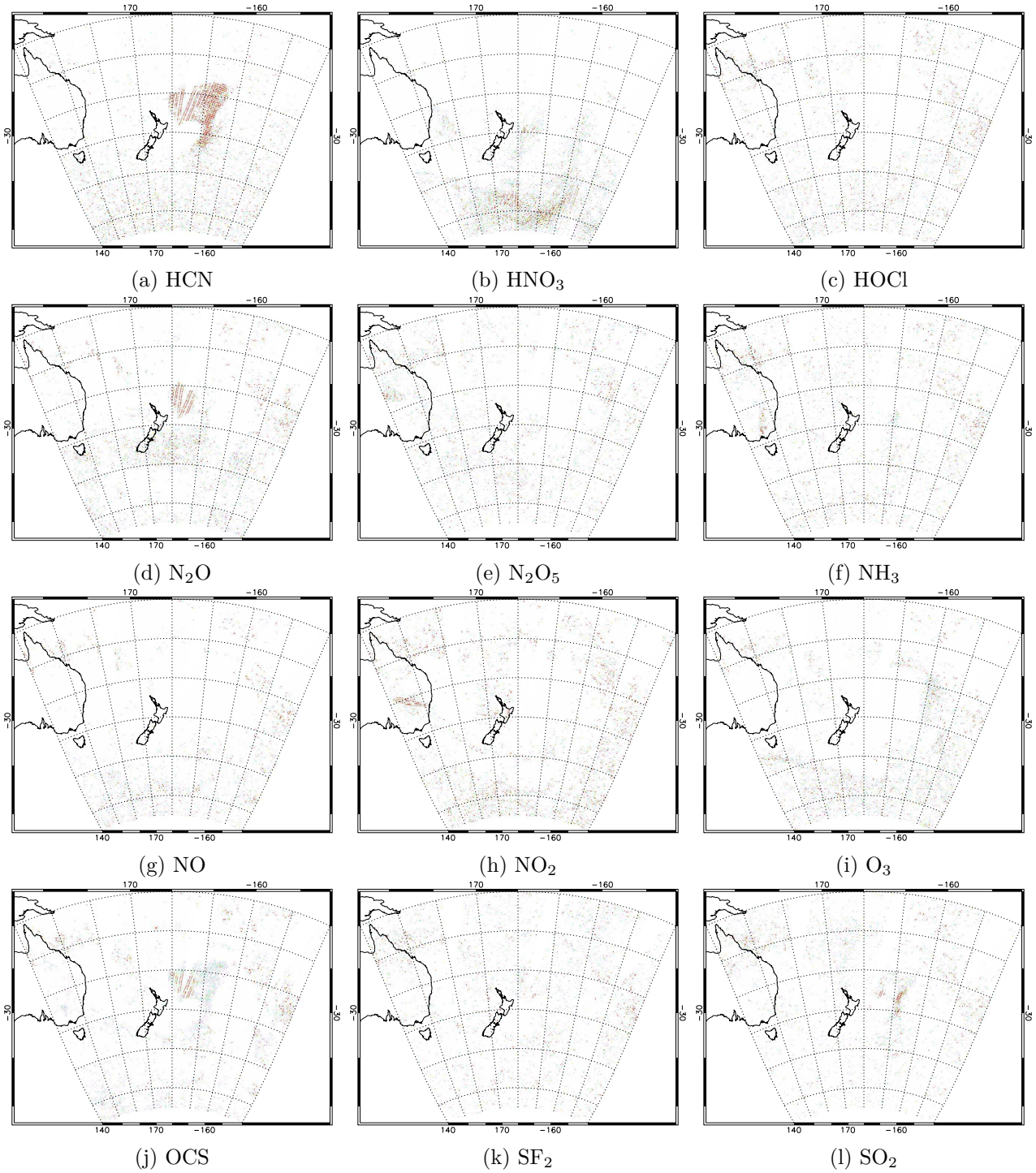

(a) HCN (b) HNO_3 (c) HOCl

(d) N_2O (e) N_2O_5 (f) NH_3

(g) NO (h) NO_2 (i) O_3

(j) OCS (k) SF_2 (l) SO_2

Figure 15: Maps of the plume on the afternoon of the 8th February 2009 for many different gases.

D Normalized Jacobian Plots

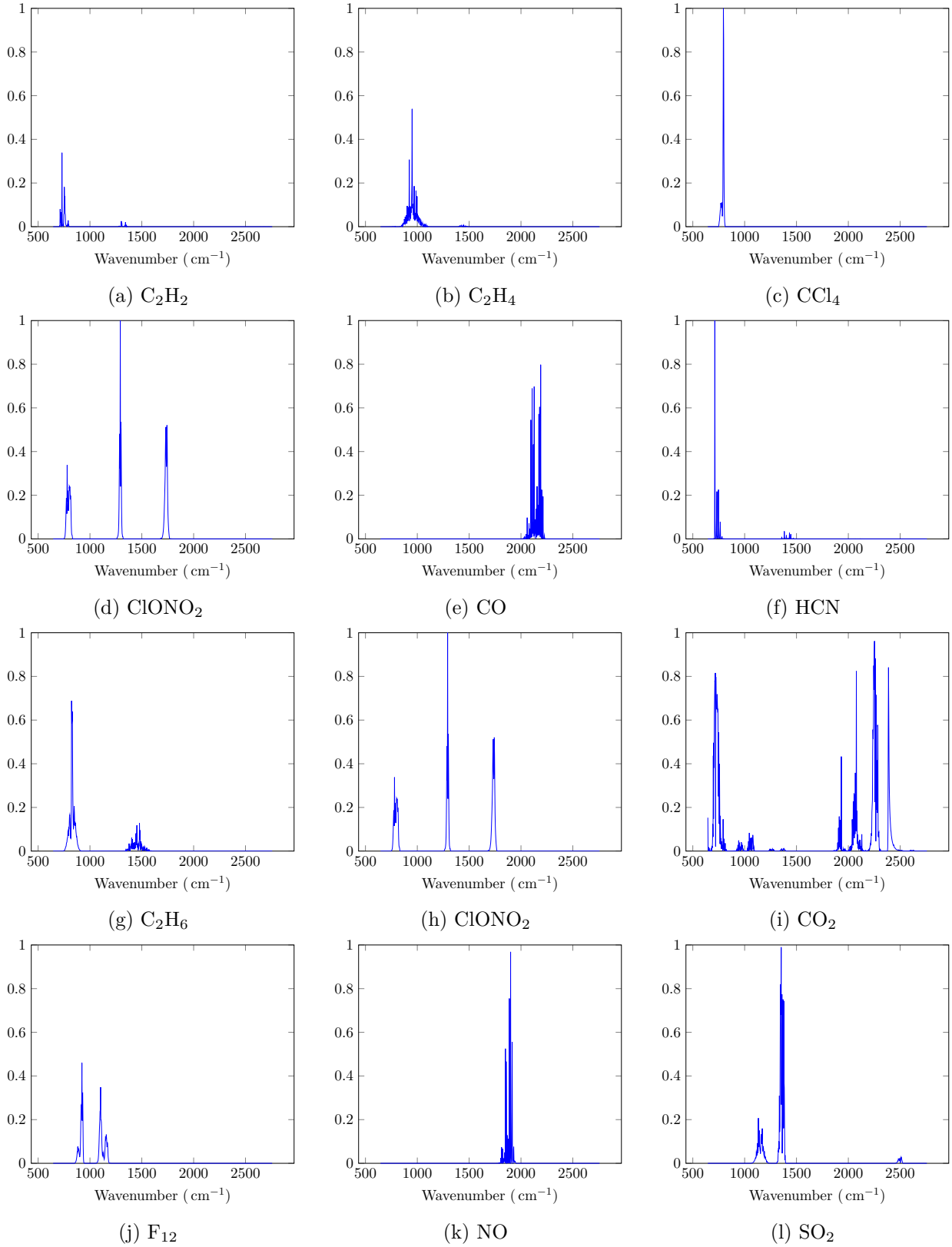

(a) C_2H_2 (b) C_2H_4 (c) CCl_4

(d) $ClONO_2$ (e) CO (f) HCN

(g) C_2H_6 (h) $ClONO_2$ (i) CO_2

(j) F_{12} (k) NO (l) SO_2

Figure 16: Normalized Jacobians for the major gases. The first six are for the biomass event, the second for the volcano.